Ganguly *et al.*
Future Journal of Pharmaceutical Sciences (2023) 9:24
https://doi.org/10.1186/s43094-023-00474-4

Future Journal of Pharmaceutical Sciences

RESEARCH Open Access

Identification of an inhibitor for atherosclerotic enzyme NOX-1 to inhibit ROS production

Rik Ganguly, Angneh Ngoruh, Prosperwell Ingty, Shashi Kumar Yadav and Atanu Bhattacharjee*

Abstract

Background NOX-1 overexpression has been observed in various studies, persons with diabetes or cardiovascular conditions. NOX-1 orchestrates the disease pathogenesis of various cardiovascular conditions such as atherosclerotic plaque development and is a very crucial biomarker. Therefore, this study was carried out to deduce the three-dimensional modelled structure of NOX-1 using DeepMind AlphaFold-2 to find meaningful insight into the structural biology. Extensive in silico approaches have been used to determine the active pocket, virtually screen large chemical space to identify potential inhibitors. The role of the key amino acid residues was also deduced using alanine scanning mutagenesis contributing to the catalytic process and to the overall stability of NOX-1.

Results The modelled structure of NOX-1 protein was validated using ERRAT. The ERRAT statistics with 9 amino acids sliding window have shown a confidence score of 96.937%. According to the Ramachandran statistics, 96.60% of the residues lie within the most favoured region, and 2.80% of residues lie in the additionally allowed region, which gives an overall of 99.4% residues in the three quadrants in the plot. GKT-831 which is a referral drug in this study has shown a GOLD interaction score of 62.12 with respect to the lead molecule zinc000059139266 which has shown a higher GOLD score of 78.07. Alanine scanning mutagenesis studies has shown that Phe201, Leu98 and Leu76 are found to be the key interacting residues in hydrophobic interactions. Similarly, Tyr324, Arg287 and Cys73 are major amino acid residues in the hydrogen bond interactions.

Conclusions NOX-1 overexpression leads to heightened ROS production resulting in catastrophic outcomes. The modelled structure of NOX-1 has a good stereochemistry with respect to Ramachandran plot. The lead molecule zinc000059139266 has shown to have a very high interaction score of 78.07 compared to the referral drug GKT-831 with a score of 62.12. There is an excellent scope for the lead molecule to progress further into in vitro and in vivo studies.

Keywords NOX-1, ROS, DeepMind, AlphaFold-2, Alanine scanning mutagenesis

Background

Atherosclerosis is an extensively studied health condition that helps in the manifestation of several different cardiovascular diseases [1]. The various inflammatory, as well as oxidative stress metabolic pathways, plays a major role in different stages of atherosclerosis. The enzyme (Nicotinamide adenine dinucleotide phosphate oxidase) NOX is associated with various problems such as atherosclerosis, oxidative stress, vascular inflammation, endothelial dysfunction, and vascular remodelling [2]. NOX-1

*Correspondence:
Atanu Bhattacharjee
atanubioinfo@gmail.com
Department of Biotechnology and Bioinformatics, North-Eastern Hill University, Umshing Mawkynroh, Shillong, Meghalaya 793022, India

induced by endotoxin expressed in the cardiomyocytes causes apoptosis, which is supported by several evidences [3]. NOX-1 is a transmembrane electron transfer protein that plays a major role in mitochondrial electron leakage leading to elevation in the catastrophic reactive oxygen species (ROS) production [4]. The function of the NOX isozymes is not only to regulate normal vascular physiology but also in abnormal conditions contribute to the development of different cardiovascular conditions including atherosclerosis [2, 5].

The NOX family consists of NOX-1 to 5 and Duox1 and 2 isoforms. Among them, the NOX-1, NOX-2, and NOX-4 isozymes are expressed in the cardiovascular tissues. Flavin adenine dinucleotide (FAD), haem and calcium ions are the essential co-factors for the proper functionality of NOX-1. NOX-1 mRNA is most abundantly expressed in colon epithelial [6], but it is also present at lower levels in vascular smooth muscle cells (VSMCs), endothelial cells, uterus, placenta, prostate, osteoclasts, retinal pericytes, neurons, astrocytes, and microglia [7–9]. NOX-1 connects with the p22phox membrane component at the protein level, which is required for enzymatic activity [10–12]. By maintaining vascular wall ROS production, inflammation, and matrix remodelling, vascular SMC plays a significant role in atherogenesis and the formation of atherosclerotic plaques [13].

NOX-1 is an inducible gene and its expression is increased in vascular cells by several pro-inflammatory stimuli including Angiotensin II (Ang II), interferon-γ (IFN-γ) and platelet-derived growth factor (PDGF) [14–17]. Interleukin-1 (IL-1) and interferon (IFN), two pro-inflammatory molecules, induce the upregulation of NOX-1 in the vascular wall under pathological circumstances associated with inflammation [18, 19]. Its levels were found to be incredibly low in atherosclerotic lesions in both humans and rabbits, whereas NOX-1 overexpression was seen in people with diabetes or cardiovascular disease [20, 21]. In a mouse atherosclerosis model, NOX-1-derived ROS changes the lesion's composition and contributes to its growth [22]. In reaction to tobacco smoke, NOX-1 raises ROS levels in VSMCs [23].

NOX-2 is crucial for innate host defence, operating as a signalling molecule to start a variety of inflammatory and immune-protective responses and creating ROS to destroy intruders following phagocytosis [24]. NOX-2 has been found to be expressed in a variety of other tissues than phagocytes, including the central nervous system, endothelium, VSMCs, fibroblasts, cardiomyocytes, skeletal muscle, hepatocytes, and hematopoietic stem cells [25]. Superoxide generated by NOX-2 can interact with NO in cells to control bioavailability, leading to the reactive molecule Peroxynitrite (ONO_2^-), which has been linked to oxidative stress. In endothelial cells, NO is a crucial signalling and vasodilator molecule. Endothelial dysfunction and hypertension are both caused by the deregulation of NOX-2 activity [26].

Based on sequence homology to gp91phox, NOX-3 was first found in 2000 along with NOX-4 and NOX-5 [27]. The three-dimensional structure of NOX-3 is anticipated to resemble that of NOX-1 and NOX-2 [25].

In comparison to other NOX enzymes, NOX-4 mRNA is substantially more prevalent in all vascular wall cells [28–31]. NOX-4 differs from NOX-1 and NOX-2 in that it creates H_2O_2 instead of O_2^-. Additionally, NOX-4 is activated during differentiation and is constitutively active rather than being triggered by inflammatory cytokines [32].

In the early phases of endothelial lesion development, the VSMCs of the intima of advanced coronary lesions express NOX-5. NOX-5 is a significant ROS generator in atherosclerosis, and it is also significant for oxidative damage. NOX-5 RNA and protein levels were shown to be considerably higher in coronary arteries of individuals with coronary heart disease compared to healthy arteries, which was also consistent with the Ca^{2+}-dependent activity of NADPH oxidase in arteries [33].

There are several different reported NOX inhibitors that are present, most of which are non-specific and can bind to the other isoforms of NOX. Very few inhibitors selectively inhibit NOX-2 such as GSK2795039 [34]. Similarly, GKT-137831 (Setanaxib/GKT-831) showed promising pharmacokinetic properties during phase one clinical trials, it inhibits NOX-1 & 4. In phase 2 clinical trial, GKT-831 succeeded in primary and secondary efficacy endpoint [35]. The NOX inhibitor APX-115 inhibits NOX-1, 2 & 4 it is safe & passed from phases 1 & 2, very effective, especially for diabetic kidney diseases [36]. In diseases like hypertrophy, cardiac remodelling & diabetes-induced atherosclerosis, setanaxib proves to be more beneficial [37].

Previously reported inhibitors such as GSK2795039 have shown a good specificity for the target protein NOX-2 but are not aqueous soluble, which will make it difficult to be available as an oral drug. Inhibitors such as GKT-137831 have shown properties related to skin and eye irritant, have solubility issues for becoming water-soluble, and have a high chance of being a P-gp substrate which can result in the involvement with the efflux system leading to inefficient drug delivery. APX-115 is a pan NOX inhibitor acting broadly on NOX-1, 2 and 4 where NOX-4 has been reported to be pro-atherosclerotic in properties. Apart from that APX-115 is dimethyl sulfoxide (DMSO) soluble and not water-soluble which makes it difficult for being orally bioavailable.

In this manuscript, we have tried to focus on NOX-1 protein due to its major role in atherosclerosis as well as various shreds of evidence that indicated the reduction of the atherosclerotic plaque in various knockout experimentations. A more specific as well as safer lead can be used as a future drug molecule as a promising NOX-1 inhibitor.

Materials and methodology

Structure deduction using Google DeepMind, AlphaFold-2

The structure of NOX-1 has not been reported in any database. Hence, the macromolecular structure for NOX-1 was deduced using Goole DeepMind AlphaFold-2, to elucidate the role and catalytic function of NOX-1. AlphaFold module of ChimeraX version 1.4 was used to visualise the structural accuracy prediction [38].

Protein secondary structure analysis

Algorithms such as ERRAT [39], PROCHECK [40], and ProtParam [41], Hydropathy index using Kyte and Doolittle [42], transmembrane region prediction using SOSUI server [43], and secondary structure analysis using GOR [44] were used to check the secondary structure as well as the overall quality of the protein model.

Retrieval of ligands and virtual screening

A set of six million three-dimensional compounds were retrieved from the ZINC database. Virtual screening was performed using the Lipinski rule of five for screening orally-bioavailable drug-like molecules. The parameters used for the primary screening of the molecules were followed according to Ganguly et al., 2022 [45]. 3 million compounds have cleared the primary filter from the initial 6 million compounds. These molecules were screened for Pharmacokinetic properties using SwissADME; only 6000 final screened molecules were used for further studies.

Prediction of the catalytic pocket for NOX-1

Computed Atlas of Surface Topography of proteins (CASTp) was used to predict the amino acid residues which are contributing to the formation of the catalytic pocket [46]. Multiple sequence alignment of NOX-1, NOX-2, NOX-3, NOX-4 and 5 with an accession ID Q9Y5S8.2, P04839.2, 056533.1, Q9NPH5, Q96PH1 were retrieved, respectively, to perform multiple sequence alignment using CLUSTALW [47] for checking the similarity in the position between the conserved domain and the active site residues.

Referral drug selection

Through the review of the literature, the compound Setanaxib (GKT-137831) [35] with a PubChem compound ID 58496428 was selected as the referral molecule against the target NOX-1. The molecular interaction score in terms of the GOLD Score was used as the threshold score for molecular interaction studies.

Protein–protein interaction (PPI) studies

Protein–Protein Interaction Networks Functional Enrichment Analysis studies were performed using STRING server to identify different interacting proteins with NOX-1.

Molecular interaction studies

Using Genetic Optimization for Ligand Docking (GOLD) version 5.2, the protein–ligand docking was carried out [48]. The protein-bound co-crystal ligand was thought to have a binding site in the form of a grid box with a radius of 6. Using the GOLD Score p450 csd docking technique, the interactions were obtained in terms of GOLD scores. A GOLD fitness score was used to determine the optimal stance. The following equation (Eq. 1) may be used to mathematically represent the GOLD fitness function [49]:

$$f = S_{\mathrm{hb_{ext}}} + S_{\mathrm{vdw_{ext}}} + S_{\mathrm{hb_{int}}} + S_{\mathrm{vdw_{int}}}$$

where the scores supplied by weak Van der Waals forces are represented by $S_{\mathrm{vdw_{ext}}}$ and $S_{\mathrm{vdw_{int}}}$. $S_{\mathrm{hb_{ext}}}$ is the hydrogen bonding score between the protein and the ligand. $S_{\mathrm{hb_{int}}}$ represents the internal hydrogen bonding of the ligand.

Selection of key amino acid residues from the molecular interactions

The most frequently repeating amino acid residues which are involved in molecular interaction with different interacting partners were searched and listed as the key amino acid residues.

Alanine scanning mutagenesis of the key amino acid residues

Alanine scanning mutagenesis was performed using I-Mutant Suite [50] which uses Support Vector Machine-based predictors. Where the change in the overall free energy of the protein in terms of protein stability was calculated based on single point mutation of the identified key amino acid residues.

Results

Protein structural analysis

The structure of NOX-1 has been deduced using AlphaFold-2, where per-residue confidence score (pLDDT) for most of the amino acid residues were ranging from 70 to 100 (Fig. 1A). The deep blue region of the predicted protein structure has a high level of confidence

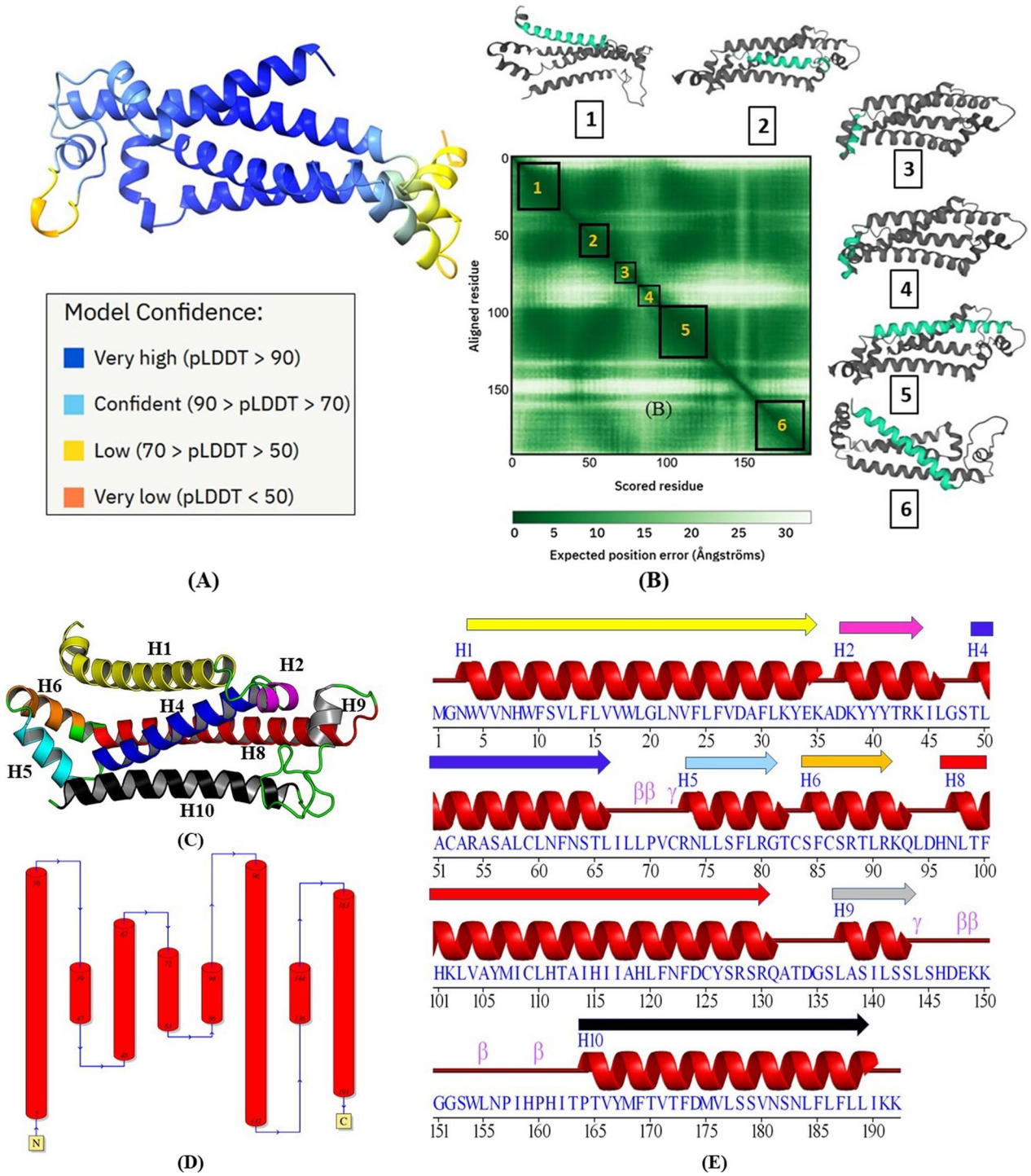

Fig. 1 Showing **A** the confidence scores related to the predicted structure of NOX-1 **B** predicted pairwise alignment error plot for AlphaFold predicted NOX-1 structure **C** all the helices present in the structure of NOX-1 **D** relative positions of the helices in the structure **E** the amino acid sequence and the relative positions of the different helices

of above 90. The light blue has a confidence of 70 to 90, yellow coloured region has a confidence of 50 to 70 and orange coloured region depicts very low level of confidence below 50. In the case of the predicted structure of NOX-1, most of the amino acid residues were found to be within the high confidence zone.

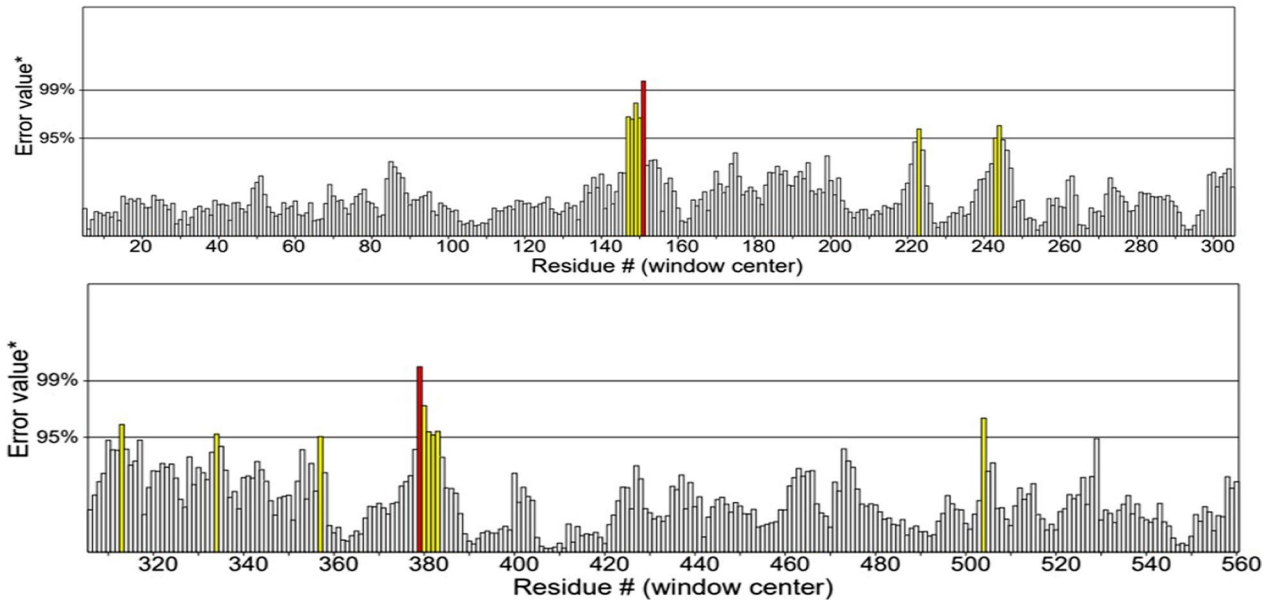

Fig. 2 Showing statistics for ERRAT algorithm, used to estimate the overall structural quality of the modelled protein NOX-1

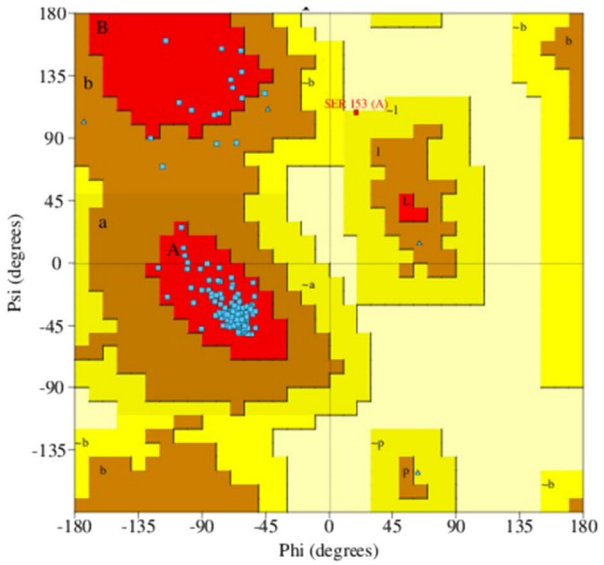

Ramachandran Plot		
1	Most favoured regions (Red coloured region)	96.60%
2	Additional allowed regions (Brown coloured region)	2.80%
3	Generously allowed regions (Yellow coloured region)	0.60%
4	Disallowed regions (Light yellow)	0.00%
	Non-glycine and non-proline residues	100.00%

(A) (B)

Fig. 3 Showing **A** torsion angle statistics of the modelled protein structure for NOX-1, **B** the details of the Ramachandran plot for NOX-1

The part of the amino acid residue in the yellow zone which represents per-residue confidence score of 50 to 70 are mainly covered by the terminal residues and the loop region. Predicted pairwise alignment error plot covers different helices present in the derived NOX-1 structure with high level of accuracy (Fig. 1B). In the predicted structure of NOX-1, there are eight helices which are connected by random coils or loops. The helices are numbered as H1, H2, H4, H5, H6, H8, H9 and H10 depicted by yellow, magenta, blue, cyan, orange, red, grey and black shown in Fig. 1C, D, F.

ERRAT is an algorithm to predict the global structural quality for the modelled protein structures. This algorithm has a sliding window of few residues and it scans the entire sequence length of a protein to analyse the outliers in the sequence with respect to an error value. The modelled structure of NOX-1 has shown an overall quality factor of 96.937% (Shown in Fig. 2) which is much

higher than 95%. The structure is considered to be good or of a high resolution if it produces the ERRAT score of 95% or higher values.

Ramachandran plot defines the distribution of the phi (ϕ) and psi (ψ) backbone torsion angles of the protein and is used in the validation of the modelled structure. The above Ramachandran plot shows (Fig. 3A) the most favoured region was found to be 96.60% (red colour), additionally allowed region is depicted by brown colour and is found to be 2.80%, yellow depicts the generously allowed regions and is found to be 0.60% and the amino acid residues were found in the disallowed region (Fig. 3B). The overall quality of the protein structure was found to be good enough for study of in silico molecular interaction.

ProtParam algorithm is used to compute various physiochemical parameters of the given protein sequence stored in Swiss-Prot or TrEMBL. The number of amino acids for NOX-1 was found to be 564 and the molecular weight was found to be 64.87104 kDa. The total number of negatively charged residues combining Arg and Glu was found to be 49. Similarly, the total number of positively charged residues combining Arg and Lys was 59. The theoretical iso-electric point (PI) is the pH where the net charge of the protein is neutral was estimated to be 8.79. The extinction coefficient indicates how much light a protein can absorb at a certain wavelength. In our study, the protein absorbance was found to be 1.770 measured at 280 nm for NOX-1, assuming all the Cysteine residues are forming disulfide bonds giving rise to Cystines. Similarly, the estimated absorbance measured at 280 nm for NOX-1, assuming all Cys residues are in their reduced state was found to be 1.754. *Half-life* (symbol t1/2) is the time required for a quantity to reduce to *half* of its initial value. ProtParam analysis for NOX-1 has shown that the estimated half-life of the protein expressed in vitro in mammalian reticulocytes will be 30 h, more than 20 h if expressed in yeast cells and more than 10 h if grown in in-vivo culture in *Escherichia coli*. The half-life of the protein NOX-1 is far more than 5 h which correlates with the estimated values for the instability index, which is a measure of proteins to determine its stability. If the index is less than 40, it is predicted to be stable or else it is unstable. NOX-1 has shown an instability index of 39.69 which indicates that the protein structure is stable. The aliphatic index of a protein is defined as the relative volume occupied by aliphatic side chains which is related to the thermostability of several group of proteins. For NOX-1 the high aliphatic index was found to be 89.70. The Grand average of hydropathicity (GRAVY) value for NOX-1 defines about the hydropathicity of a protein, which is defined based on the group of hydrophobic residues in a sequence. NOX-1 has shown a gravy value of 0.022. Hydropathy index of the protein indicates the presence of a transmembrane region. From the hydropathy index plot using Kyte and Doolittle (Fig. 4), it is clear that the regions such as 0–30, 100–120, 160–200, 200–220 and 275–290 of the amino acid sequence match with the hydropathy charge plot from SOSUI server prediction (Fig. 5). Therefore, there is high confidence in the prediction of the transmembrane segments.

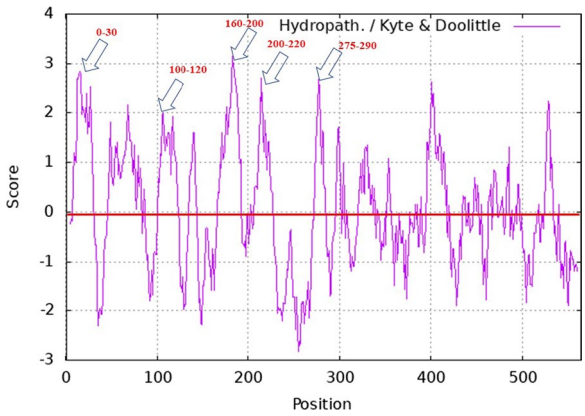

Fig. 4 Showing hydropathy index for NOX-1

Active pocket determination and multiple sequence alignment

The active pocket of the deduced protein structure for NOX-1 was identified utilising the surface topology search for the derived structure. The major cleft or pocket is considered to be the main active pocket by the CASTp algorithm, where the highest surface area of the pocket was found to be 2563.307 $Å^2$ and the volume was found to be 2343.249 $Å^3$. Multiple sequence alignment algorithm (Shown in Additional file 1: Figure S1) of different isoform of NOX (NOX-1 to 5) has given several conserved domains and most of it are coinciding with the active site computed by CASTp (Fig. 6).

Protein–protein interaction studies

The Protein–Protein *Interaction* Networks Functional Enrichment Analysis was performed using STRING server [51]. The NOX-1 (red coloured is the central protein) is shown to interact with other proteins. The two nodes connected by yellow line shows text mining, light blue line shows protein homology, green line represent gene neighbourhood, pink line shows gene fusions, blue line represent gene co-occurrence, cyan line depicts from curated databases and purple depicts experimental determined. The maximum interrelation of NOX-1 is with NADPH oxidase Organizer 1 (NOXO1) which is

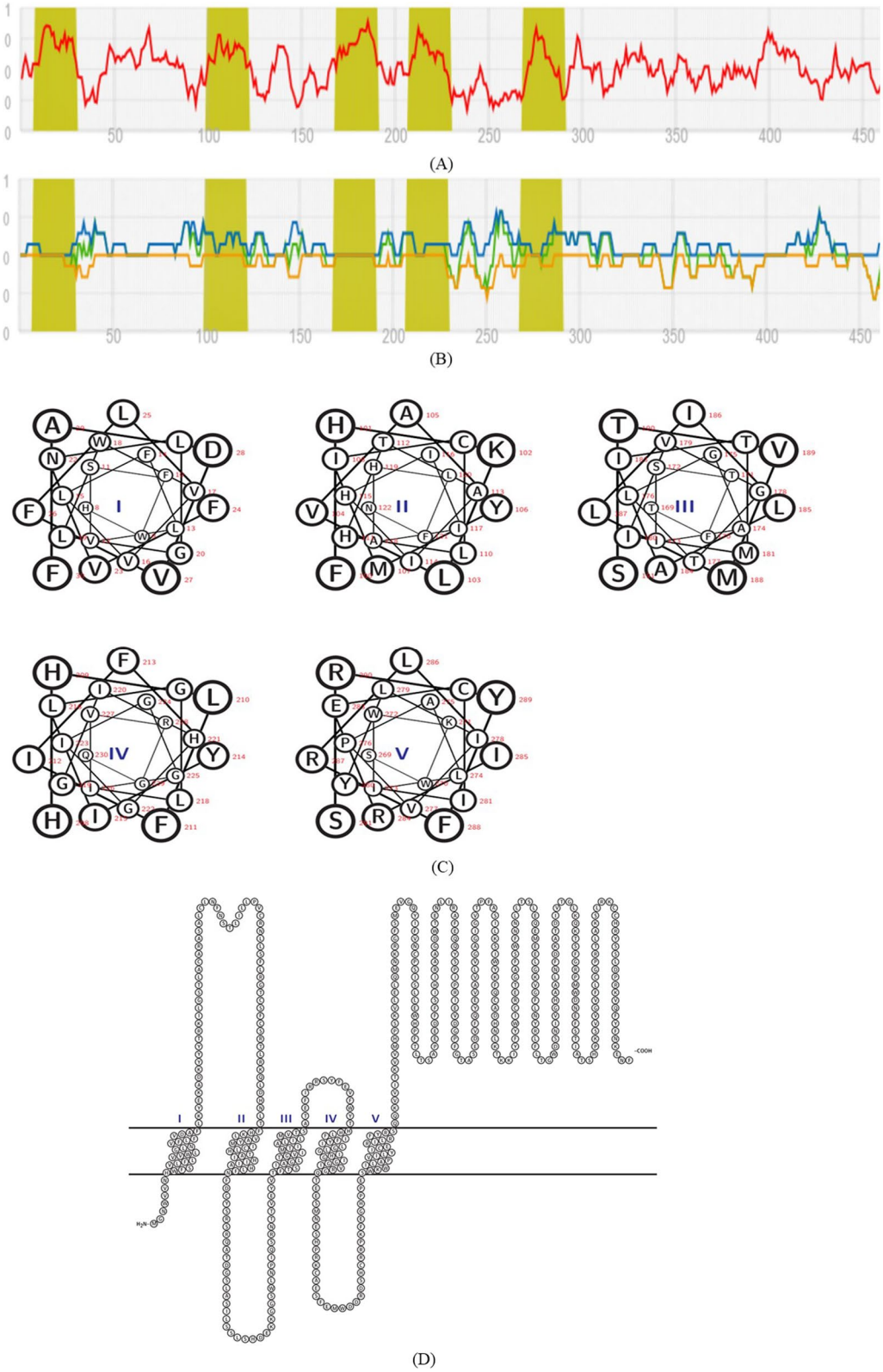

Fig. 5 Showing **A** hydropathy plot for NOX-1 from SOSUI server, **B** charge plot for NOX-1 from SOSUI server, **C** wheel plot of transmembrane helices for NOX-1, **D** snake like plot for transmembrane region for NOX-1

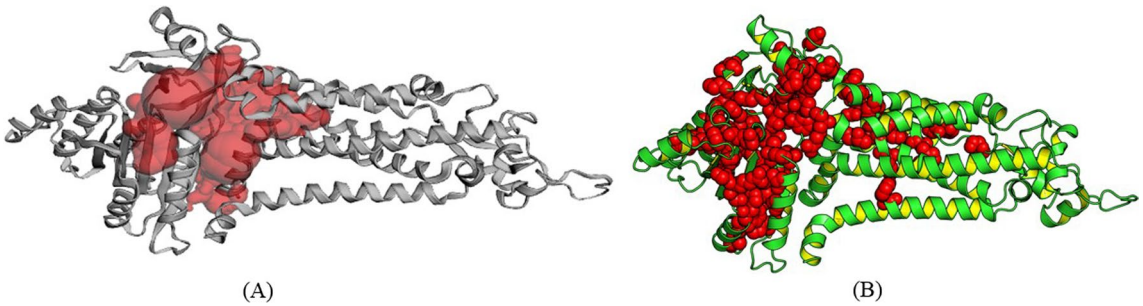

Fig. 6 Showing **A** surface topology map of NOX-1 where the active pocket is shown in red coloured cloud representation, **B** the conserved region of the NOX-1 protein from multiple sequence alignment

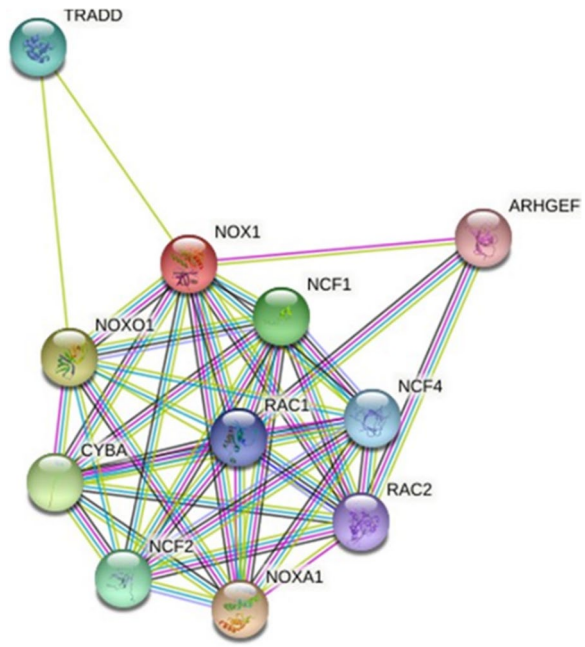

Fig. 7 Showing protein–protein network interactome map with NOX-1

a regulatory subunit of NOX-1 and positively regulates NOX-1 and NOX-3 [52] followed by Ras related c3 botulinum toxin substrate1 (RAC1). RAC1 activates NOX-1 and triggers ROS generation, cytochrome b-245 light chain (CYBA) associates with NOX-3 generate superoxides [53], Ras related c3 botulinum toxin substrate2 (RAC2) is a GTPase membrane bound protein helps in phagocytosis, cell polarization and ROS generation [54], NOXA1 is a regulatory subunit of NOX-1 [55] and Neutrophil cytosol factor 2 (NCF2) neutrophil NADPH oxidase, activates NOX-2 [56] (Fig. 7).

Molecular interaction studies

The results of the molecular interaction showed that the referral drug Setanaxib/GKT-831 interact with the amino acid residues Val71, Arg73, Phe201, His209, Phe211, Tyr280, Arg287, Phe326, Trp337 and Asp382 by hydrophobic interaction and the amino acid residue Arg284 interacts the referral drug GKT-831 by hydrogen bond interaction with a GOLD Score of 62.12 (Shown in Fig. 8A, B). A compound zinc000059139266 has shown a GOLD Score of 78.0745 and it interacts with the amino acid residues Leu76, Ser77, Arg80, Asn97, Leu98, Thr387, Glu562 and Phe564 through hydrophobic interaction. Arg73, Asp95, Tyr324, Gly386, Ala388 and Asn563 through hydrogen bond (Shown in Fig. 8C, D). The GOLD Score of the lead compound zinc000062716991 is 77.3351 and is interacting with the amino acid residues Phe201, Phe326, Trp337 and Asp382 by hydrophobic interaction and Arg73, Arg284, Arg287 amino acid residues is interacting through a hydrogen bond (Shown in Fig. 8E, F). A lead compound zinc000005413557 has a GOLD Score of 74.5633 (Shown in Fig. 8G, H) and is interacting with the amino acid residues Arg73, Trp205, His208, His209, Ser291, Phe326, Trp337 and Asp382 by hydrophobic interaction and Arg284, Arg287 through a hydrogen bond (Shown in Table 1).

Identification of the key amino acid residues

Key amino acid residues are the active pocket amino acid residues that were found to be frequently occurring in several molecular interaction studies with the referral as well as the lead-like molecules. This key amino acid residue from all the top scoring molecular interactions was found to be Val71, Arg73, Leu76, Ser77, Arg80, Asp95, Asn97, Leu98, Phe201, Trp205, His208, His209, Arg284, Arg287, Tyr324, Phe326, Trp337, Asp382, Gly386, Thr387, Glu562, Asn563 and Phe564. These amino acid residues were further subjected to alanine scanning mutagenesis to understand the importance of these key residues in the contribution to the binding pocket to maintain the overall stability of the NOX-1 (Table 2).

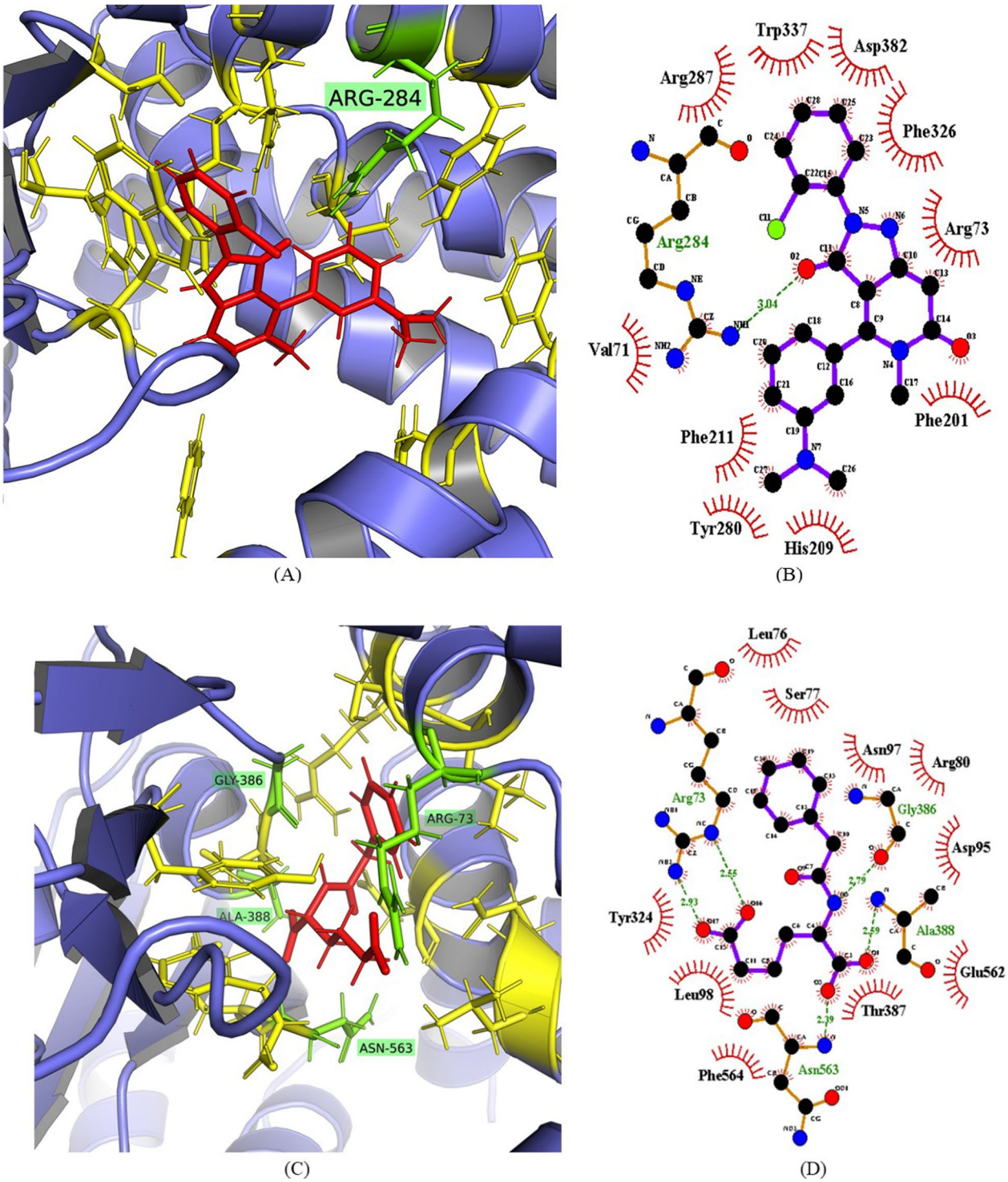

Fig. 8 Showing the spatial arrangement of the interacting residue in three-dimensional space in (**A**), (**C**), (**E**) and (**G**), where the ligand molecule is shown in red, amino acids involved in hydrophobic interaction in yellow and hydrogen bond interaction in green. Similarly, the two-dimensional representation of the molecular interaction between nox-1 and **B** Setanaxib/GKT-831, **D** zinc000059139266, **F** zinc000062716991 and **H** zinc000005413557 are shown, where the hydrogen bond interaction is represented by the green dotted lines and the amino acid residues involved in hydrogen bond interaction is shown using red coloured eyelashes

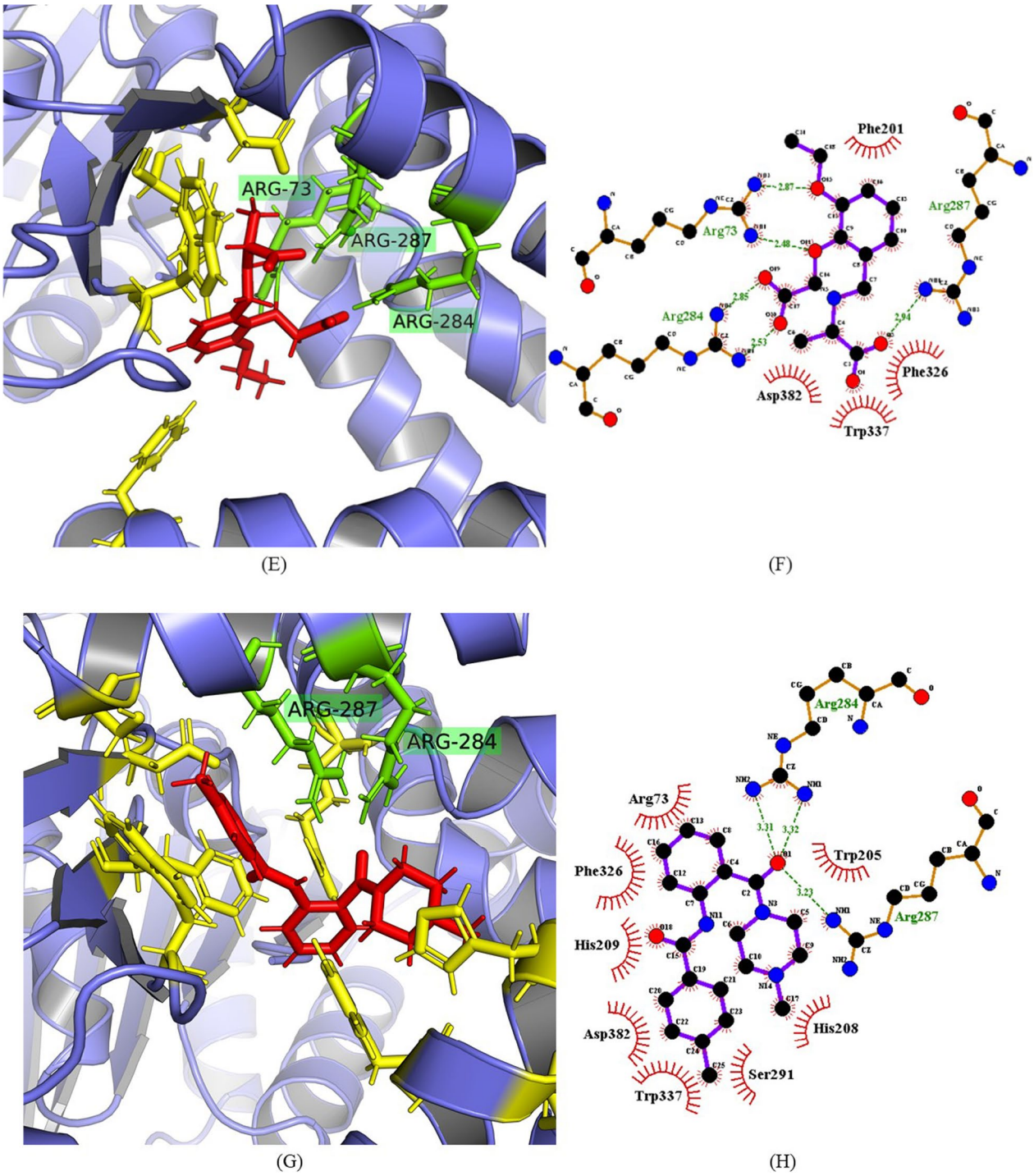

Fig. 8 continued

Alanine scanning mutagenesis

The site-directed mutagenesis method known as "alanine scanning" is used in molecular biology to identify the impact of a specific amino acid residue on the global stability or functionality of a given protein. In all the different protein–ligand interactions between NOX-1 and the various top-scoring lead-like molecules, there were eighteen amino acid residues that were found to be frequently interacting with the heteroatom or ligand (Shown in Additional file 1: Table S2.).

Table 1 Showing results of the molecular interaction studies

Sl no.	Receptor	Small molecule	AA-HBI*	AA-HPI**	Gold score
1	Nox-1	Setanaxib/GKT-831	Arg284	Val71, Arg73, Phe201, His209, Phe211, Tyr280, Arg287, Phe326, Trp337, Asp382	62.12
2	Nox-1	zinc000059139266	Arg73, Gly386, Ala388, Asn563	Leu76, Ser77, Arg80, Asp95, Asn97, Leu98, Tyr324, Thr387, Glu562, Phe564	78.07
3	Nox-1	zinc000062716991	Arg73, Arg284, Arg287	Phe201, Phe326, Trp337, Asp382	77.33
4	Nox-1	zinc000005413557	Arg284, Arg287	Arg73, Trp205, His208, His209, Ser291, Phe326, Trp337, Asp382	74.56

AA-HBI*, amino acid residue involved in hydrogen bond interaction; AA-HPI**, amino acid residue involved in hydrophobic interaction

Table 2 Showing the atom pairs involved in hydrogen bond formation and their relative atomic distances

Sl. no.	Interacting atoms	Atom name (from ligand)	HB donor/acceptor	AA name from receptor	HB donor/acceptor	Atomic distance (in Å)
1	Zinc59139266 & NOX-1	O-1 of ligand	Donor	Ala388 (N–H group)	Acceptor	2.9
		N-5 of ligand	Acceptor	Gly386 (C=O group)	donor	2.8
		O-3 of ligand	Donor	Asn563 (N–H group)	Acceptor	2.4
		O-16 of ligand	Donor	Arg73 (N–H group)	Acceptor	2.5
		O-17 of ligand	Donor	Arg73 (N–H group)	Acceptor	2.9
2	Setanaxib/GKT-831 & NOX-1	O-2 of ligand	Donor	Arg284 (N–H group)	Acceptor	3.04
3	zinc000062716991 & NOX-1	O-11 of ligand	Donor	Arg73 (N–H group)	Acceptor	2.5
		O-15 of ligand	Donor	Arg73 (N–H group)	Acceptor	2.9
		O-19 of ligand	Donor	Arg284 (N–H group)	Acceptor	2.8
		O-20 of ligand	Donor	Arg284 (N–H group)	Acceptor	2.5
		O-3 of ligand	Donor	Arg287 (N–H group)	Acceptor	2.9
4	zinc000005413557 & NOX-1	O-1 of ligand	Donor	Arg28 4 (N–H group)	Acceptor	3.3
		O-1 of ligand	Donor	Arg284 (N–H group)	Acceptor	3.3
		O-1 of ligand	Donor	Arg287 (N–H group)	Acceptor	3.2

Similarly, there are six amino acid residues found to be frequently interacting with the heteroatom or ligand (Shown in Additional file 1: Table S3).

Alanine scanning mutagenesis of all the key amino acid residues has shown that amino acid residues such as Phe201, Leu98 and Leu76 which contribute mostly to hydrophobic interactions, which when mutated to Ala is giving rise to a ΔΔG value of a Gibbs Free energy change of − 2.31, − 3.0 and − 2.85 kcal/mol (Fig. 9A). Similarly, within the six key amino acid residues involved in hydrogen bonding the ΔΔG value or a Gibbs Free energy change of the major three were found to be Tyr324, Arg287 and Cys73 with a ΔΔG value of − 1.9, − 1.01 and − 0.89 kcal/mol, respectively (Fig. 9B).

Discussion

NOX-1 has a central role in the ROS production and oxidative stress pathways which makes it an important biomarker for drug discovery. Due to the limitations in the structural availability for NOX-1, before AlphaFold-2 came into existence it was difficult to perform accurate Insilco studies. In this study, the structure of NOX-1 has been deduced using AlphaFold-2. Subsequently, the errors in the structure have been evaluated with ERRAT program which compares the derived structure with high resolution crystal structures and gives an error value. ERRAT statistics with 9 amino acids sliding window have shown a confidence score of 96.937%. Ramachandran statistics for the torsion angles in the macromolecular structure of NOX-1 have been deduced and it is observed that 96.60% of the residues lie in the most favoured region, and 2.80% of residues lie in the additionally allowed region, which gives an overall of 99.4%

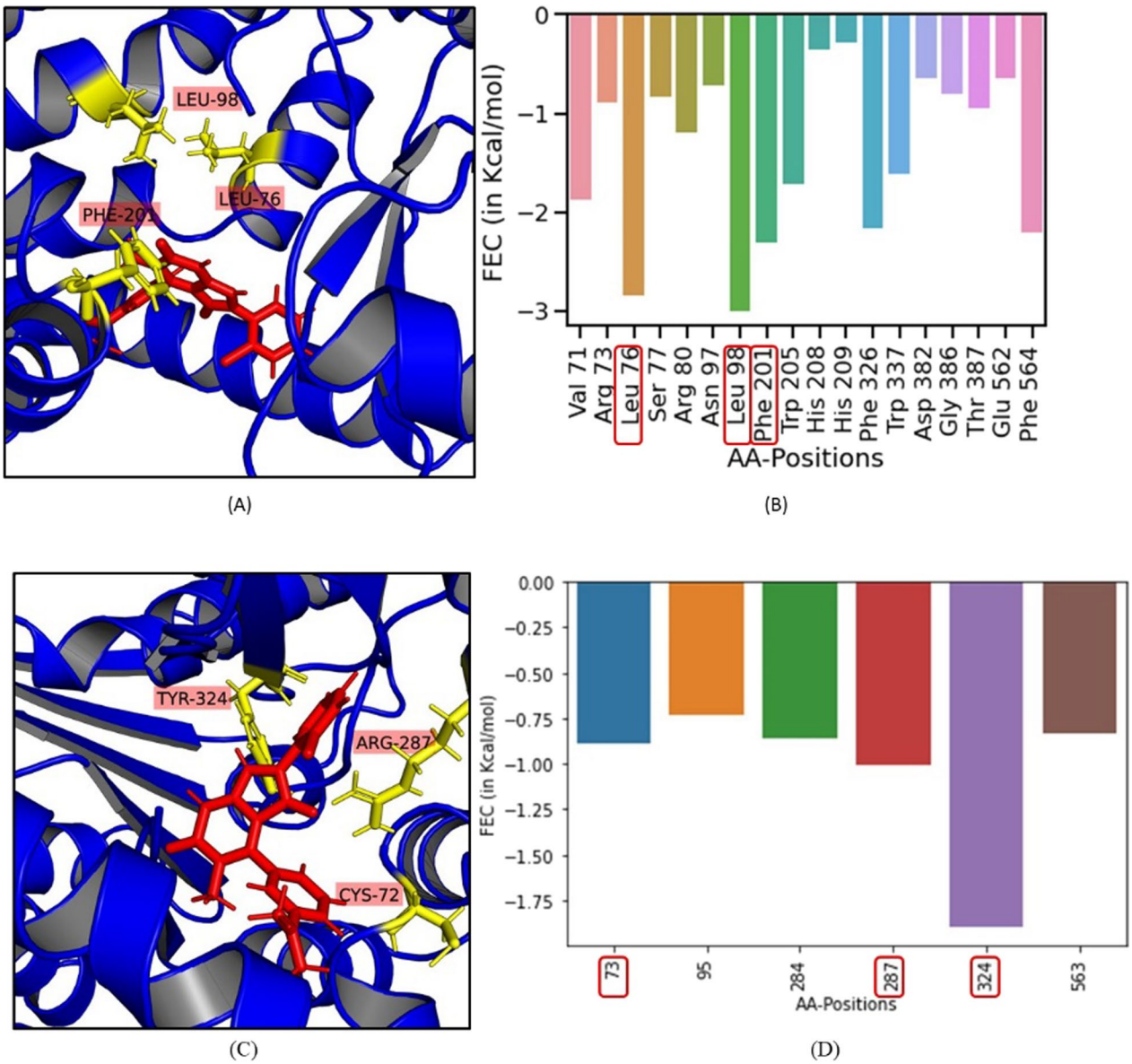

Fig. 9 Showing **A** the positions of the amino acid residues Phe201, Leu98 and Leu76 in NOX-1, **B** Alanine scanning mutagenesis for the key amino acid residues responsible for hydrophobic interactions, **C** the positions of the amino acid residues Tyr324, Arg287 and Cys73 in NOX-1, **D** alanine scanning mutagenesis for the key amino acid residues responsible for hydrogen bond interactions

residues in the three quadrants in the plot. The instability index and the GRAVY values indicate that the protein is stable. Setanaxib/GKT-831 was used as the referral drug for Insilco molecular interaction studies. GKT-831 has shown a GOLD interaction score of 62.12 with respect to that the lead molecule zinc000059139266 which has shown a higher GOLD score of 78.07. In alanine scanning mutagenesis, we have considered eighteen amino acid residues that are present in the active pocket of NOX-1 involved in hydrophobic interactions with several lead molecules. Similarly, there were six amino acid residues in the active pocket of NOX-1 involved in hydrogen bond interactions. Among all active pocket amino acid residues Phe201, Leu98 and Leu76 are found to be the key residues in hydrophobic interactions. Similarly, Tyr324, Arg287 and Cys73 are major amino acid residues in the hydrogen bond interactions. Changes in these amino acid residues with alanine have shown an adverse effect on the global stability of the protein structure. These substitutions may impede the binding of substrate to NOX-1 leading to its alteration in its function.

Conclusion

NOX-1-dependent oxidative stress, which promotes atherosclerosis, is a potential target for diabetic vasculopathy. Other pathogenic roles of NOX-1 include a mechanism of hyperoxia-induced tissue injury. In the absence of the reference NOX-1 protein structure, an attempt has been made to use DeepMind based Alpha-Fold-2 derived macromolecular structure for in silico drug discovery process. The Discovery of a potential lead molecule that can impede the normal functionality of the NOX-1 protein can open new therapeutic options. GKT-831 which is a known inhibitor for NOX-1 has shown a GOLD interaction score of 62.12. Compared to that the lead molecule zinc000059139266 has shown a better score of 78.07. Therefore, this lead molecule can be further studied in in vitro experimentations for further validation.

Abbreviations

NOX	Nicotinamide adenine dinucleotide phosphate oxidase
ROS	Reactive oxygen species
FAD	Flavin adenine dinucleotide
VSMC	Vascular smooth muscle cells
IFN-γ	Interferon-γ
PDGF	Platelet-derived growth factor
IL-1	Interleukin-1
DMSO	Dimethyl sulfoxide
CASTp	Computed Atlas of Surface Topography of proteins
GOLD	Genetic optimization for ligand docking
RAC1	Ras related c3 botulinum toxin substrate1
CYBA	Cytochrome b-245 light chain
NCF2	Neutrophil cytosol factor 2

Supplementary Information

The online version contains supplementary material available at https://doi.org/10.1186/s43094-023-00474-4.

Additional file 1. Supplementary data.

Acknowledgements

The authors acknowledge gratefully the Department of Biotechnology and Bioinformatics for providing the necessary infrastructure for carrying out the computational work and high computing facility provided by the Computer Centre, NEHU.

Author contributions

RG, AN, PI and SKY contributed to the data acquisition, data interpretation and framing the manuscript. The author AB has contributed as a research supervisor to design the research hypothesis, proof reading and final correction of the manuscript. All authors read and approved the final manuscript.

Funding

The authors of this research did not receive any funding concerning this research.

Availability of data and materials

Data and material are available upon request.

Declarations

Ethics approval and consent to participate

Not applicable.

Consent for publication

Not applicable.

Competing interests

The authors have no conflict of interest.

Received: 15 September 2022 Accepted: 19 March 2023
Published online: 28 March 2023

References

1. Rozanski A, Blumenthal JA, Kaplan J (1999) Impact of psychological factors on the pathogenesis of cardiovascular disease and implications for therapy. Circulation 99(16):2192–2217
2. Lassègue B, San Martín A, Griendling KK (2012) Biochemistry, physiology, and pathophysiology of NADPH oxidases in the cardiovascular system. Circ Res 110(10):1364–1390
3. Waghela BN, Vaidya FU, Agrawal Y, Santra MK, Mishra V, Pathak C (2021) Molecular insights of NADPH oxidases and its pathological consequences. Cell Biochem Funct 39(2):218–234
4. Zeeshan HMA, Lee GH, Kim HR, Chae HJ (2016) Endoplasmic reticulum stress and associated ROS. Int J Mol Sci 17(3):327
5. Sorescu D, Weiss D, Lassègue B, Clempus RE, Szöcs K, Sorescu GP, Valppu L, Quinn MT, Lambeth JD, Vega JD, TaylorWR GKK (2002) Superoxide production and expression of nox family proteins in human atherosclerosis. Circulation 105(12):1429–1435
6. Rokutan K, Kawahara T, Kuwano Y, Tominaga K, Nishida K, Teshima-Kondo S (2008) Nox enzymes and oxidative stress in the immunopathology of the gastrointestinal tract. Semin Immunopathol 30(3):315–327
7. Cui XL, Brockman D, Campos B, Myatt L (2006) Expression of NADPH oxidase isoform 1 (NOX1) in human placenta: involvement in preeclampsia. Placenta 27(4–5):422–431
8. Lee NK, Choi YG, Baik JY, Han SY, Jeong DW, Bae YS, Kim N, Lee SY (2005) A crucial role for reactive oxygen species in RANKL-induced osteoclast differentiation. Blood 106(3):852–859
9. Sorce S, Krause KH (2009) NOX enzymes in the central nervous system: from signaling to disease. Antioxid Redox Signal 11(10):2481–2504
10. Ambasta RK, KumarP GKK, Schmidt HH, Busse R, Brandes RP (2004) Direct interaction of the novel Nox proteins with p22phox is required for the formation of a functionally active NADPH oxidase. J Biol Chem 279(44):45935–45941
11. Hanna IR, Hilenski LL, Dikalova A, Taniyama Y, Dikalov S, Lyle A, Quinn MT, Lassègue B, Griendling KK (2004) Functional association of NOX1 with p22phox in vascular smooth muscle cells. Free Radic Biol Med 37(10):1542–1549
12. Kawahara T, Ritsick D, Cheng G, Lambeth JD (2005) Point mutations in the proline-rich region of p22phox are dominant inhibitors of NOX1- and Nox2-dependent reactive oxygen generation. J Biol Chem 280(36):31859–31869
13. Doran AC, Meller N, McNamara CA (2008) Role of smooth muscle cells in the initiation and early progression of atherosclerosis. Arterioscler Thromb Vasc Biol 28(5):812–819
14. Lassègue B, Sorescu D, Szöcs K, Yin Q, Akers M, Zhang Y, Grant SL, Lambeth JD, Griendling KK (2001) Novel gp91(phox) homologues in vascular smooth muscle cells: NOX1 mediates angiotensin II-induced superoxide formation and redox-sensitive signaling pathways. Circ Res 88(9):888–894
15. Manea A, Tanase LI, Raicu M, Simionescu M (2010) Jak/STAT signaling pathway regulates NOX1 and nox4-based NADPH oxidase in human aortic smooth muscle cells. Arterioscler Thromb Vasc Biol 30(1):105–112
16. Briones AM, Tabet F, Callera GE, Montezano AC, Yogi A, He Y, Quinn MT, Salaices M, Touyz RM (2011) Differential regulation of NOX1, Nox2 and Nox4 in vascular smooth muscle cells from WKY and SHR. J Am Soc Hypertens JASH 5(3):137–153

17. Pérez-Girón JV, Palacios R, Martín A, Hernanz R, Aguado A, Martínez-Revelles S, Barrús MT, Salaices M, Alonso MJ (2014) Pioglitazone reduces angiotensin II-induced COX-2 expression through inhibition of ROS production and ET-1 transcription in vascular cells from spontaneously hypertensive rats. Am J Physiol Heart Circ Physiol 306(11):H1582–H1593
18. Martín A, Pérez-Girón JV, Hernanz R, Palacios R, Briones AM, Fortuño A, Zalba G, Salaices M, Alonso MJ (2012) Peroxisome proliferator-activated receptor-γ activation reduces cyclooxygenase-2 expression in vascular smooth muscle cells from hypertensive rats by interfering with oxidative stress. J Hypertens 30(2):315–326
19. Aguado A, Fischer T, Rodríguez C, Manea A, Martínez-González J, Touyz RM, Hernanz R, Alonso MJ, Dixon DA, Briones AM, Salaices M (2016) Hu antigen R is required for NOX-1 but not NOX-4 regulation by inflammatory stimuli in vascular smooth muscle cells. J Hypertens 34(2):253–265
20. Schröder K (2014) NADPH oxidases in redox regulation of cell adhesion and migration. Antioxid Redox Signal 20(13):2043–2058
21. Gray SP, Di Marco E, Kennedy K, Chew P, Okabe J, El-Osta A, Calkin AC, Biessen EA, Touyz RM, Cooper ME, Schmidt HH, Jandeleit-Dahm KA (2016) Reactive oxygen species can provide atheroprotection via NOX4-dependent inhibition of inflammation and vascular remodeling. Arterioscler Thromb Vasc Biol 36(2):295–307
22. Sheehan AL, Carrell S, Johnson B, Stanic B, Banfi B, Miller FJ Jr (2011) Role for NOX1 NADPH oxidase in atherosclerosis. Atherosclerosis 216(2):321–326
23. Chang KH, Park JM, Lee CH, Kim B, Choi KC, Choi SJ, Lee K, Lee MY (2017) NADPH oxidase (NOX) 1 mediates cigarette smoke-induced superoxide generation in rat vascular smooth muscle cells. Toxicol In Vitro Int J Publ Assoc BIBRA 38:49–58
24. Rada B, Hably C, Meczner A, Timár C, Lakatos G, Enyedi P, Ligeti E (2008) Role of Nox2 in elimination of microorganisms. Semin Immunopathol 30(3):237–253
25. Bedard K, Krause KH (2007) The NOX family of ROS-generating NADPH oxidases: physiology and pathophysiology. Physiol Rev 87(1):245–313
26. Jung O, Schreiber JG, Geiger H, Pedrazzini T, Busse R, Brandes RP (2004) gp91phox-containing NADPH oxidase mediates endothelial dysfunction in renovascular hypertension. Circulation 109(14):1795–1801
27. Cheng G, Cao Z, Xu X, van Meir EG, Lambeth JD (2001) Homologs of gp91phox: cloning and tissue expression of Nox3, Nox4, and Nox5. Gene 269(1–2):131–140
28. Clempus RE, Sorescu D, Dikalova AE, Pounkova L, Jo P, Sorescu GP, Schmidt HH, Lassègue B, Griendling KK (2007) Nox4 is required for maintenance of the differentiated vascular smooth muscle cell phenotype. Arterioscler Thromb Vasc Biol 27(1):42–48
29. Ago T, Kitazono T, Ooboshi H, Iyama T, Han YH, Takada J, Wakisaka M, Ibayashi S, Utsumi H, Iida M (2004) Nox4 as the major catalytic component of an endothelial NAD(P)H oxidase. Circulation 109(2):227–233
30. Haurani MJ, Cifuentes ME, Shepard AD, Pagano PJ (2008) Nox4 oxidase overexpression specifically decreases endogenous Nox4 mRNA and inhibits angiotensin II-induced adventitial myofibroblast migration. Hypertension 52(1):143–149
31. Miller AA, Drummond GR, Schmidt HH, Sobey CG (2005) NADPH oxidase activity and function are profoundly greater in cerebral versus systemic arteries. Circ Res 97(10):1055–1062
32. Montezano AC, Burger D, Ceravolo GS, Yusuf H, Montero M, Touyz RM (2011) Novel Nox homologues in the vasculature: focusing on Nox4 and Nox5. Clin Sci 120(4):131–141
33. Guzik TJ, Chen W, Gongora MC, Guzik B, Lob HE, Mangalat D, Hoch N, Dikalov S, Rudzinski P, Kapelak B, Sadowski J, Harrison DG (2008) Calcium-dependent NOX5 nicotinamide adenine dinucleotide phosphate oxidase contributes to vascular oxidative stress in human coronary artery disease. J Am Coll Cardiol 52(22):1803–1809
34. Hirano K, Chen WS, Chueng AL, Dunne AA, Seredenina T, Filippova A, Rutter AR (2015) Discovery of GSK2795039, a novel small molecule NADPH oxidase 2 inhibitor. Antioxid Redox Signal 23(5):358–374
35. Zeng SY, Yang L, Yan QJ, Gao L, Lu HQ, Yan PK (2019) NOX1/4 dual inhibitor GKT-137831 attenuates hypertensive cardiac remodelling associating with the inhibition of ADAM17-dependent proinflammatory cytokines-induced signalling pathways in the rats with abdominal artery constriction. Biomed Pharmacother 109:1907–1914
36. Kwon G, Uddin MJ, Lee G, Jiang S, Cho A, Lee JH, Lee SR, Bae YS, Moon SH, Lee SJ, Cha DR, Ha H (2017) A novel pan-Nox inhibitor, APX-115, protects kidney injury in streptozotocin-induced diabetic mice: possible role of peroxisomal and mitochondrial biogenesis. Oncotarget 8(43):74217–74232
37. Jiao W, Ji J, Li F, Guo J, Zheng Y, Li S, Xu W (2019) Activation of the Notch-Nox4-reactive oxygen species signaling pathway induces cell death in high glucose-treated human retinal endothelial cells. Mol Med Rep 19(1):667–677
38. Goddard TD, Huang CC, Meng EC, Pettersen EF, Couch GS, Morris JH, Ferrin TE (2018) UCSF ChimeraX: meeting modern challenges in visualization and analysis. Protein Sci 27(1):14–25
39. Dym O, Eisenberg D, Yeates TO (2012) ERRAT
40. Laskowski RA, MacArthur MW, Moss DS, Thornton JM (1993) PROCHECK: a program to check the stereochemical quality of protein structures. J Appl Crystallogr 26(2):283–291
41. Garg VK, Avashthi H, Tiwari A, Jain PA, Ramkete PW, Kayastha AM, Singh VK (2016) MFPPI—multi FASTA ProtParam interface. Bioinformation 12(2):74
42. Kyte J, Doolittle RF (1982) A simple method for displaying the hydropathic character of a protein. J Mol Biol 157(1):105–132
43. Hirokawa T, Boon-Chieng S, Mitaku S (1998) SOSUI: classification and secondary structure prediction system for membrane proteins. Bioinformatics 14(4):378–379
44. Sen TZ, Jernigan RL, Garnier J, Kloczkowski A (2005) GOR V server for protein secondary structure prediction. Bioinformatics 21(11):2787–2788
45. Ganguly R, Mylliemngap BJ, Bhattacharjee A (2022) Discovery of a novel inhibitor against urokinase-type plasminogen activator, a potential enzyme with a role in atherosclerotic plaque instability. J Biomol Struct Dyn 1–11. https://doi.org/10.1080/07391102.2022.2051742
46. Tai W, He L, Zhang X, Pu J, Voronin D, Jiang S, Du L (2020) Characterization of the receptor-binding domain (RBD) of 2019 novel coronavirus: implication for development of RBD protein as a viral attachment inhibitor and vaccine. Cell Mol Immunol 17(6):613–620
47. Thompson JD, Gibson TJ, Higgins DG (2003) Multiple sequence alignment using ClustalW and ClustalX. Curr Protoc Bioinform 1:2–3
48. Verdonk ML, Cole JC, Hartshorn MJ, Murray CW, Taylor RD (2003) Improved protein–ligand docking using GOLD. Proteins Struct Funct Bioinform 52(4):609–623
49. Kang L, Li H, Jiang H, Wang X (2009) An improved adaptive genetic algorithm for protein–ligand docking. J Comput Aided Mol Des 23(1):1–12
50. Capriotti E, Fariselli P, Casadio R (2005) I-Mutant2.0: predicting stability changes upon mutation from the protein sequence or structure. Nucleic Acids Res 33(Web Server issue):W306–W310
51. Szklarczyk D, Franceschini A, Wyder S, Forslund K, Heller D, Huerta-Cepas J, Von Mering C (2015) STRING v10: protein–protein interaction networks, integrated over the tree of life. Nucleic Acids Res 43(D1):D447–D452
52. Choi DH, Cristóvão AC, Guhathakurta S, Lee J, Joh TH, Beal MF, Kim YS (2012) NADPH oxidase 1-mediated oxidative stress leads to dopamine neuron death in Parkinson's disease. Antioxid Redox Signal 16(10):1033–1045
53. Ueno N, Takeya R, Miyano K, Kikuchi H, Sumimoto H (2005) The NADPH oxidase Nox3 constitutively produces superoxide in a p22phox-dependent manner: its regulation by oxidase organizers and activators. J Biol Chem 280(24):23328–23339
54. Knaus UG, Heyworth PG, Evans T, Curnutte JT, Bokoch GM (1991) Regulation of phagocyte oxygen radical production by the GTP-binding protein Rac 2. Science 254(5037):1512–1515
55. Cheng G, Ritsick D, Lambeth JD (2004) Nox3 regulation by NOXO1, p47phox, and p67phox. J Biol Chem 279(33):34250–34255
56. Giardino G, Cicalese MP, Delmonte O, Migliavacca M, Palterer B, Loffredo L, Cirillo E, Gallo V, Violi F, Pignata C (2017) NADPH oxidase deficiency: a multisystem approach. Oxid Med Cell Longev 2017:4590127

Publisher's Note